Phase Space of Binary Black Holes from Gravitational Wave Observations to Unveil its Formation History

Samsuzzaman Afroz 61,* and Suvodip Mukherjee 61,†

¹Department of Astronomy and Astrophysics, Tata Institute of Fundamental Research, Mumbai 400005, India

Gravitational Wave (GW) sources offer a valuable window to the physical processes that govern the formation of binary compact objects (BCOs). However, deciphering such information from GW data is substantially challenging due to the difficulty in mapping from the space of observation to the space of numerous theoretical models. We introduce the concept of BCO Phase-Space that connects the observable space to the evolution trajectories of the BCO formation channels with cosmic time and apply it to the third GW transient catalog (GWTC-3) that brings new insights into probable astrophysical formation scenarios of nearly 90 events. Our study reveals that two events, GW190425 and GW230529, show an overlap with a BCO Phase Space trajectory of the same formation channel arising from a sub-solar mass black hole scenario that has grown into a higher mass by accretion, hinting towards the common primordial origin of both these sources. Though the actual formation channel is yet to be confirmed, with the availability of more GW events, the BCO Phase Space can delve into distinguishing features of different formation channels for both astrophysical and primordial origin and opens the possibility of bringing new and deeper insights on the formation and evolution of BCOs across all observable masses over most of the cosmic time.

Introduction: The study of gravitational wave (GW) events has opened a transformative window into our understanding of the universe, allowing us to probe the origins and evolution of binary compact objects (BCOs) [1, 2]. These BCOs encode crucial information about their formation processes and evolutionary histories, making it essential to extract and analyze this information to enhance our understanding of binary evolution [3–8]. With availability of a few tens of high signal-tonoise ratio GW events [9–18], the traditional methods for inferring the population of the GW sources, which is primarily by combining the posteriors of different samples and has been successful in shedding light on the mass distribution and merger rate distribution of the binary compact objects. But the main physics question remains unknown, that is what are the different formation channels though binary compact objects form, and how do they evolve over the cosmic time?

To answer the above-mentioned astrophysical question, we need to understand the mapping between the space of the formation channels of compact objects with the space of GW observations. The mapping between these two spaces can connect the formation and evolution history of binaries with the correlations between observable quantities in the GW data. In this work, we propose a new approach the BCO Phase Space which can capture the evolution track of different formation scenarios of BCOs in terms of the observable quantities of the GW sources such as masses, spins, luminosity distance, eccentricity, kick velocity, or any other observable [106]. The observed GW events capture different regions in the BCO Phase Space and its overlap with the trajectories may be able to identify the possible formation channel. Each formation channel whether resulting from isolated binary evolution, dynamical interactions in dense star clusters, or primordial origins leads to distinct trajectories in this phase space. More importantly, BCO Phase Space enables us to identify not only known formation channels, but also any new population of the GW sources that can exist in nature, but not predicted by any simulations.

This method provides a more nuanced perspective on the underlying processes both of astrophysical and primordial origin that influence the formation and evolution of binary systems.

We demonstrate this new BCO Phase Space technique on the 90 events from GWTC-3 [11] along with GW230529 [19] from the fourth observation run detected by the LIGO[20]-Virgo[21]-KAGRA[22] (LVK) collaboration to get an insight on the formation channel of the compacts objects with the possibility for both astrophysical and primordial origin. We identify possible overlap of these events with the astrophysical formation channel scenarios arising from the first generation, second generation, and mergers in AGN disc for these binary black holes (BBHs) demonstrating what are their possibilities of overlapping with different formation channels. In this work, we only focus on the BBHs scenario and do not consider the neutron star. The BCO Phase Space of a neutron star will exhibit very complementary and rich information about the system. So we plan to consider it in a separate work. We consider all the low mass events except GW170817 [23] in the analysis for finding its overlap with the BCO Phase Space of BBH origin (for both astrophysical and primordial scenario). This is because the true nature of these sources (black hole or neutron star) cannot be confirmed until independent observation such as electromagnetic counterparts [24, 25] or tidal deformation [26, 27] are made.

Characterizing Formation Pathways for Primordial black holes through Phase Space: PBHs are potential sources of GW that could be detected by current and future GW observatories [28–30]. Further details on the merger rate for PBHs used in this analysis are given in Appendix A. The merger rate of PBHs with redshift gets mapped to a merger rate with luminosity distance (D_L) . Depending on different formation scenarios of PBHs [31–34], the growth of a PBH mass is significantly influenced by its initial mass distribution at the time of formation. Over time, however, PBHs can increase in mass through the accretion of matter [35, 36].

The maximum rate at which a PBH can accrete matter is defined by the Eddington limit, which balances gravitational attraction with radiation pressure. The mass accretion rate can be expressed as [37]:

$$\dot{M} = \dot{m}\dot{M}_{\rm Edd} = \dot{m} \times 2.2\,{\rm M}_{\odot}/{\rm Gyrs}\left(\frac{M}{{\rm M}_{\odot}}\right),$$
 (1)

where $\dot{M}_{\rm Edd}$ represents the Eddington accretion rate, M denotes the mass of the PBH, and \dot{m} is the mass accretion index. For PBHs with very low initial masses on the order of $10^{-5} M_{\odot}$ and high mass accretion rates, the final masses can grow to values within the range of current GW detector sensitivity within the age of the universe. Conversely, higher initial masses of the order of 1 M_{\odot} with lower accretion rates can also result in final masses that fall within the detectable range of GW observations.

A value of $\dot{\rm m}=1$ corresponds to the Eddington accretion rate, while values less than 1 indicate sub-Eddington accretion. Additionally, there is a relationship between mass accretion and spin [38]. As PBHs accrete matter, their spin increases due to the angular momentum gained from the infalling material. The spin parameter, χ , evolves from an initial value of zero to a maximum of one, depending on the redshift z and the mass accretion rate $\dot{\rm m}$. We parametrize the spin parameter, χ , as a function of redshift z and mass accretion rate $\dot{\rm m}$, given by the following equation:

$$\chi(z, \dot{m}) = 1 - e^{-k \cdot \dot{m} \cdot \Delta t}, \qquad (2)$$

where Δt is the time difference (measured in Gyrs) between the initial redshift $z_{\rm initial}$ and the current redshift z, and k is a constant controlling the rate of spin evolution. Different values of k lead to varying spin growth rates.

The GW events are generated by sampling mass and spin values from their respective distributions using the inverse CDF method. The total number of GW events is then calculated using Equation (6), assuming a PBH fraction of $f_{\rm pbh}=0.001$ and an observation period of 26 months. For the mass distributions, we utilize lognormal distributions (defined in Appendix A), with the characteristic mass evolving as a function of redshift according to Equation (1). The standard deviation is set at 2% of the characteristic mass. Similarly, for the spin distribution, we use the mean value defined in Equation (2), adding 2% Gaussian noise. From these sampled values, we calculate the chirp mass and effective spin, and the resulting events are plotted in phase space.

Characterizing Formation Pathways for Astrophysical Black Holes through Phase Space: ABHs are believed to form through several key channels[107]: isolated binary evolution [39–41], dynamical interactions in dense stellar environments [42–44], and hierarchical mergers [45, 46]. Understanding these formation pathways is crucial for accurate astrophysical modeling and theoretical predictions.

Isolated Binary: In the isolated binary evolution channel, black holes form from the collapse of massive stars

within binary systems, without significant external influences from surrounding environments. This channel typically produces first-generation (1G) black holes, with masses determined by stellar evolution processes. Specifically, the pair-instability supernova mechanism limits the masses of 1G black holes to approximately 45-50 M_{\odot} [47]. Black holes formed through this mechanism tend to have low to moderate spins (though it is not a smoking gun feature), which are influenced by the rotation of their progenitor stars and the efficiency of angular momentum transfer during stellar collapse. In isolated binary systems, black hole formation can be accompanied by mass transfer or common envelope phases, which affect the final masses and spins of the resulting black holes. For the merger rate distribution in luminosity distance, we use the merger rate model in redshift constructed using Madau-Dickinson star formation rate (SFR) model [48] with a delay time distribution [49–52].

Hierarchical Mergers: Hierarchical mergers refer to the process in which black holes formed from earlier mergers undergo further mergers with other black holes, resulting in higher-generation black holes. In this study, we focus primarily on second-generation (2G) black holes, which are direct products of first-generation black hole mergers (1G+1G). These 2G black holes emerge when two 1G black holes merge, allowing them to surpass the mass limits imposed by stellar evolution, particularly the pair-instability mass gap. Unlike black holes formed through stellar collapse, 2G black holes retain around 95% of the combined mass of their progenitor black holes [53, 54]. Additionally, these black holes tend to have higher spins, typically clustering around a spin parameter of 0.7, as a result of the merger dynamics [55– 57]. For 2G black holes, the delay time model is assumed from the merger rate of first-generation BBHs. So, we consider a delay time distribution model with respect to the 1G mergers, as discussed in the Appendix C. This causes the 2G merger rate to be suppressed and shifted to lower redshifts, as expected, as shown in Figure 6. Although the BCO Phase Space can be constructed for any merger rate scenario, we have kept a simplistic model for this first application of BCO Phase Space.

Dynamical Interactions in Dense Stellar Environments: Dynamical evolution channels involve environments where black holes form and merge through gravitational interactions within dense stellar or gas-rich regions. These environments include globular clusters [58, 59], nuclear star clusters, young star clusters [60], and AGN disks. In this study, we focus specifically on BBHs in AGN disks within the dynamical environment and will consider other formation channels in future work. We discussed the AGN formation scenario in more details in the Appendix D. For each of these scenarios, there are theoretical estimates of the BBH properties which can be explored using simulations [61–65]. In this work, we consider a parametric form to explore different formation scenarios in the BCO Phase Space. However, it can be easily extended to specific theoretical models based on simulations.

Construction of the BCO Phase Space: To gener-

ate the phase space for ABHs and PBHs, we divide the redshift range from z=0 to z=4 into 160 bins of size 0.025. The total number of GW events is calculated using Equation (6) for each population based on their respective merger rates. We generate GW events by sampling mass and spin values from their distributions using the Cumulative distribution function (CDF) method. From these samples, we compute the chirp mass and effective spin, plotting the resulting events in phase space, as shown in Figure 1.

For the generation of the phase space (Figure 1), we have used the following parameter values for mass distribution, which is parameterized by a combination of Gaussian and exponential decay functions (defined in Appendix B): for 1G black holes, $M_{mean} = 8$ M_{\odot} , $\sigma = 1.5 M_{\odot}$, and $\alpha = 0.15$; for 2G black holes, $M_{mean} = 16 M_{\odot}, \ \sigma = 2.0 M_{\odot}, \ and \ \alpha = 0.06; \ and for$ black holes in AGN disks, $M_{\rm mean} = 30 \ M_{\odot}, \ \sigma = 2.5 \ M_{\odot},$ and $\alpha = 0.05$ to allow for a broader mass spectrum, as shown in Figure 4. For the spin parameter, due to limited observational knowledge, we parameterize the spin as a function of mass which can capture a wide range of spin behaviors (defined in Appendix B), and is illustrated in Figure 5. For 1G and AGN disk black holes, we use this parametrization with the following parameter values: $m_{\min} = 5M_{\odot}$, $m_{\max} = 120M_{\odot}$, n = 1.0, $\beta = 0.2$, and $\gamma = 0.01$. For 2G black holes, we assume a Gaussian distribution centered at a spin of 0.7 with a standard deviation of 0.1. We have varied some parameters that have the most significant impact on the phase space to better analyze and infer information about the formation channels. In our study, we assume a delay time of 500 Myrs for 1G black holes and 1 Gyrs for 2G black holes (detailed in Appendix C). For the merger rate of BBHs in AGN disks, we utilize the description provided in [66], which is detailed in Appendix D.

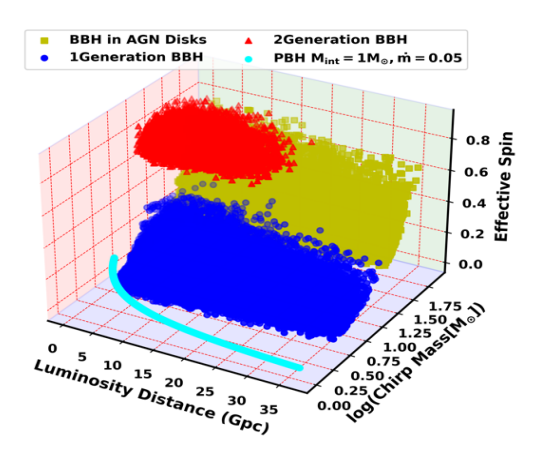


FIG. 1: This 3D plot illustrates the phase space distribution of ABHs and PBHs, highlighting the distribution of chirp mass, luminosity distance, and effective spin parameter. It shows the distinct regions in the phase space occupied by 1G black holes, 2G black holes, black holes formed in AGN disks, and PBHs.

In this phase space, overlaps may occur in some regions between BBHs in AGN disks and 2G BBHs, as well as between AGN black holes and 1G black holes.

This degeneracy can be resolved by introducing a fourth parameter: eccentricity. Isolated binary evolution generally results in nearly circular orbits due to mass loss from stellar winds and GW emission [67]. In contrast, binaries formed through dynamical interactions can retain higher eccentricities, especially during close encounters. Hierarchical mergers can also yield eccentric orbits depending on the dynamics involved [68]. Current GW observatories like LIGO primarily measure the dominant (2,2)modes, which are associated with nearly circular orbits and provide limited information about eccentricity. Higher-order modes that may indicate eccentricity are not dominant signals and fall within a frequency range where current detector sensitivity is insufficient. However, future detectors with enhanced sensitivity could measure these higher-order modes, enabling more effective differentiation between formation channels.

Finding Black Hole formation channels from the GWTC-3 Catalog: In this study, we analyze the phase space of observed GW events using the GWTC-3 catalog [11], along with the publicly available event GW230529 [19]. Each event provides measurements of several key parameters that shape the waveform of the GW signal. For this study, we focus on three primary parameters: M_c , χ_{eff} , and D_L . Using the posterior distributions of these parameters for each event, we construct a three-dimensional phase space, as detailed in Appendix E. This phase space framework allows us to examine how different formation models project onto the observed data.

In this study, we focus on two key parameters that significantly influence the shape of the phase space trajectories for both PBHs and ABHs. For PBHs, these parameters are the mass accretion rate index, m, and the initial mass, $M_{\rm int}$. In the case of ABHs, we consider three distinct formation channels: 1G BBHs, 2G BBHs, and BBHs forming in AGN disks. For 1G BBHs and those formed in AGN disks, we vary the spin parameter denoted by n and the mean of the Gaussian mass distribution denoted by M_{mean} (See Appendix B for more details.). For 2G BBHs, we explore both the mean mass, M_{mean} , and the mean spin parameter, χ_{mean} , as the spin distribution for 2G BBHs is assumed to follow a Gaussian distribution. By systematically varying key parameters for each of the four cases: PBHs, 1G BBHs, 2G BBHs, and AGN disk BBHs we explore a wide range of the phase space. For 1G BBHs, we vary the mean mass $(M_{\rm mean})$ from 5 to 12 M_{\odot}, for 2G BBHs from 15 to 30 M_{\odot} , and for BBHs in AGN disks from 20 to 40 M_{\odot} . The spin parameter (n) is varied from 0.6 to 1.5 for 1G BBHs, and from 0.5 to 1.5 for BBHs in AGN disks. We also vary the mean spin (χ_{mean}) from 0.30 to 0.70 for 2G BBHs. For PBHs, the initial mass $(M_{\rm int})$ ranges from 10^{-3} to 1 M_{\odot}, and the accretion rate (\dot{m}) spans from 0 to 1, covering sub-Eddington to Eddington limits. We fix the spin evolution parameter k for PBHs to 10, and for ABH spin cases, we set $\beta = 0.8$ and $\gamma = 0.04$ due to their minimal impact on trajectories. This broad parameter space serves as a prior in the likelihood analysis, enabling the generation of diverse phase space trajecto-

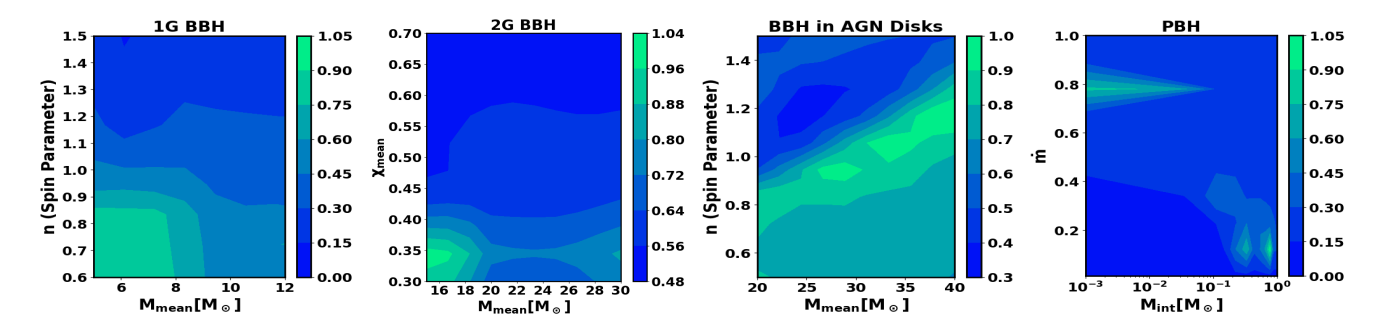


FIG. 2: P Projection of phase space trajectories for different BBH formation channels. Leftmost: 1G BBHs, illustrating the probability of phase space trajectories generated by variations in the spin parameter n and the mean mass M_{mean} . Second from the left: 2G BBHs, highlighting the probability associated with variations in the mean mass M_{mean} and the mean spin parameter χ_{mean} , assuming a Gaussian distribution for the spin. Third from the left: Binary black holes formed in AGN disks, depicting the probability of trajectories influenced by variations in the spin parameter n and the mean mass M_{mean} . Rightmost: PBHs, showcasing the probability of their trajectories within the phase space based on the mass accretion rate index m and the initial mass M_{int} . The color bar in all plots represents the probability value.

ries.

We then project these trajectories onto the BCO Phase Space derived from observed GW events. A detailed description of the underlying framework is mentioned in Appendix F. We calculate the selection function, as not all events in a given trajectory fall within the LVK detection band. The selection function is computed using mass and distance, as these are the most sensitive parameters for detecting events. For each parameter combination across the four cases (1G, 2G, BBHs in AGN disks, and PBH), we calculate the probability of the selection-function-weighted trajectories as follows:

$$P_{\rm trajectories} = \sum_{\tilde{r}_i \in \rm trajectories} Z(\tilde{r}_i), \tag{3}$$

here, $P_{\rm trajectories}$ represents the total probability of the selection-function-weighted trajectories, where \tilde{r}_i denotes the coordinates of BCO events in phase space which are allowed by the selection function for a given detector sensitivity and observation time. The summation is carried out over all points that belong to the selection-function-weighted trajectories, and $Z(\tilde{r}_i)$ is the phase space weight at each coordinate \tilde{r}_i .

The probability results for the four scenarios are presented in Figure 2. For 1G BBH, these probabilities suggest that it is more likely to have a low mean mass and a shallow spin growth n < 1 value. This arises as most of the sources in the GWTC-3 indicate low mass and non-spinning. In contrast, for BBHs in AGN disks, a higher mean mass M_{mean} and slightly higher values of n are more probable, suggesting there can be significant growth of spin. This arises due to a few GW events with heavier mass and non-zero spin. For the 2G BBH formation channel, the results are less conclusive, as the phase space regions that exhibit higher probabilities can show significant degeneracy with other channels. However, if we ignore this degeneracy, slightly higher mean masses (around $M_{mean} = 16 M_{\odot}$) with a mean spin around $\chi_{\rm mean} = 0.35$ appear to be somewhat more probable than other combinations.

In the case of PBHs, the probability is generally very low across most regions in the parameter space. However, certain regions offer some support for PBHs. One such region is for PBHs with masses close to 0.1 to 1 M_{\odot} and low accretion rates (around $\dot{m} \sim 0.1$). This is supported by observations of low-redshift, low-mass, and high-spin events. Additionally, another region that provides support involves PBHs with initial masses between 0.001 and 0.01 M_{\odot} and high accretion rates (around $\dot{m} \sim 0.8$), which align with events characterized by chirp masses of $\sim 30~{\rm M}_{\odot}$ at redshifts around 0.9. This low support is arising because the PBH trajectory differs from the ABH trajectory, but at higher masses (as shown in Figure 1), there can be degeneracy with 2G and AGN black holes at high masses. It is important to note these constraints are completely independent of any constraints feasible from the stochastic GW background [69-71].

Six such events in the catalog are unlikely to originate from the standard ABH formation channels considered in this paper, as they all have relatively lower masses. Among these, GW190425 and GW230529 are particularly notable due to their significantly high spins, which matches with a possible hypothesis that these have undergone accretion, making them possible candidates for further investigation as PBHs. To further explore the potential PBH origin of these events, we provide the specific combinations of M_{int} and m for which each event individually falls along a PBH trajectory in the BCO Phase Space in Figure 11. For the two standout events, GW230529 and GW190425, we present six combinations of initial masses, accretion rates, and spin parameters (k) in Table I for which both events overlap within the 68% C.I. of their respective posteriors.

An alternative explanation for these events could be the formation of second-generation BBHs from the merger of two neutron stars, heavy neutron stars, or any exotic compact objects, or this may be viewed in light of the uncertainties regarding core collapse supernovae and fallback efficiency [72, 73], as well as the systematics inherent in the GW side [74–76]. In the future, exploration of the BCO Phase Space for neutron stars (or exotic compact objects) along with PBHs will shed

Parameters	Case-1	Case-2	Case-3	Case-4	Case-5	Case-6
$ m M_{int}$	0.0100	0.0703	0.1306	0.1708	0.2311	0.3115
m	0.18	0.11	0.09	0.08	0.07	0.06
k	7	8	9	10	10	11

TABLE I: The table lists six combinations of initial PBH masses ($M_{\rm int}$), accretion rates \dot{m} , and spin parameters (k), each corresponding to a distinct trajectory in the PBH phase space that is consistent with both the GW230529 and GW190429 events within the 68% C.I.

more light on such possibilities with the availability of more events by identifying which of these trajectories is getting more occupied with GW sources.

In addition to this BCO Phase Space analysis in terms of mass parameters, we classify the GW events in the catalog (excluding GW170817, which has been confirmed as a binary neutron star system due to its observed electromagnetic counterpart [23]). This classification is presented in Figure 11 in the Appendix F. For each event, we assign a probability indicating whether it originates from 1G binaries or from a combined category of 2G+AGN scenario. Events with a low probability of originating from either of these channels are highlighted in gray within the pie chart, indicating these as confusing sources that may be potential PBH candidates or neutron stars, or BBHs from mergers of two 1G neutron stars. If the probability is sufficiently high for either 1G or the combined 2G + AGN category, the event is marked in black. This demonstrates the impact of this new BCO Phase Space technique to explore different formation channels from GW data.

Conclusions: In this work, we introduced a novel framework for identifying the formation channels of BCOs such as neutron stars and black holes by leveraging the phase space geometry of GW events. Our method offers a flexible, data-driven approach by directly analyzing the phase space trajectories that represent different BCO formation channels. Each formation channel has distinct characteristics, placing it in a unique region of the phase space. By projecting these theoretical trajectories onto the observed phase space, we demonstrate that it is possible to infer key information related to the formation channels of the BCOs detected.

By applying this technique to the GWTC-3 catalog and GW230529 we explore different physical scenarios of formation associated with these binaries. Our findings show that most of the GW events are classified in first-generation and second-generation scenarios, except six events which are in the mass gap (as shown in Figure 11 in Appendix-F). A closure inspection reveals that two events GW190425 and GW230529 can be associated with a common origin of a sub-solar black hole which has gone through a similar sub-Eddington accretion to grow into a mass and spin with which it is detected by the GW detectors. Though this finding from BCO Phase Space analysis is only an initial hint, other possible astrophysical scenarios of low mass-gap events are yet to be explored. However in the future with more detected GW events, it will be possible to distinguish whether more

low-mass events are appearing on the PBH trajectory or ABH trajectory. Either way, this new revelation using BCO Phase Space will make a paradigm shift in our understanding of the formation and evolution of compact objects.

As BCO Phase Space can capture any scenarios of formation channel (known or unknown), it will be possible to make serendipitous discoveries of new formation scenarios of either astrophysical or primordial origin using this technique. With the future LVK observations, this BCO Phase Space technique will be extended for neutron stars, and globular clusters formation scenarios and will also be extended for its application on future GW detectors such as Cosmic Explorer [77], Einstein Telescope [78], and LISA [79], along with the inclusion of other observables such as eccentricity and kick velocity. These advanced detectors, with their ability to measure wider frequency ranges, will provide significantly improved accuracy that will enable more precise characterization of binary formation channels and will bring deeper insights on their formation and cosmic evolution.

Acknowledgments

The authors express their gratitude to Michela Mapelli for reviewing the manuscript and providing useful comments as a part of the LIGO publication policy. This work is part of the \data|theory\ Universe-Lab, supported by TIFR and the Department of Atomic Energy, Government of India. The authors express gratitude to the system administrator of the computer cluster of \data|theory\ Universe-Lab and the TIFR computer center HPC facility for computing resources. Special thanks to the LIGO-Virgo-KAGRA Scientific Collaboration for providing noise curves. LIGO, funded by the U.S. National Science Foundation (NSF), and Virgo, supported by the French CNRS, Italian INFN, and Dutch Nikhef, along with contributions from Polish and Hungarian institutes. This collaborative effort is backed by the NSF's LIGO Laboratory, a major facility fully funded by the National Science Foundation. The research leverages data and software from the Gravitational Wave Open Science Center, a service provided by LIGO Laboratory, the LIGO Scientific Collaboration, Virgo Collaboration, and KAGRA. Advanced LIGO's construction and operation receive support from STFC of the UK, Max-Planck Society (MPS), and the State of Niedersachsen/Germany, with additional backing from the Australian Research Council. Virgo, affiliated with the European Gravitational Observatory (EGO), secures funding through contributions from various European institutions. Meanwhile, KAGRA's construction and operation are funded by MEXT, JSPS, NRF, MSIT, AS, and MoST. This material is based upon work supported by NSF's LIGO Laboratory which is a major facility fully funded by the National Science Foundation. We acknowledge the use of the following packages in this work: Numpy [80], Scipy [81], Matplotlib [82], and Astropy [83].

- * Electronic address: samsuzzaman.afroz@tifr.res.in
 † Electronic address: suvodip@tifr.res.in
- M. Bailes et al. Gravitational-wave physics and astronomy in the 2020s and 2030s. Nature Rev. Phys., 3(5):344–366, 2021.
- [2] Makoto Arimoto et al. Gravitational Wave Physics and Astronomy in the nascent era. 4 2021.
- [3] Michela Mapelli. Formation Channels of Single and Binary Stellar-Mass Black Holes. 2021.
- [4] Giuliano Iorio et al. Compact object mergers: exploring uncertainties from stellar and binary evolution with SEVN. 11 2022.
- [5] Floor S. Broekgaarden et al. Impact of Massive Binary Star and Cosmic Evolution on Gravitational Wave Observations II: Double Compact Object Rates and Properties. 12 2021.
- [6] Jim W. Barrett, Sebastian M. Gaebel, Coenraad J. Neijssel, Alejandro Vigna-Gómez, Simon Stevenson, Christopher P. L. Berry, Will M. Farr, and Ilya Mandel. Accuracy of inference on the physics of binary evolution from gravitational-wave observations. *Mon. Not. Roy. Astron. Soc.*, 477(4):4685–4695, 2018.
- [7] Michal Dominik, Krzysztof Belczynski, Christopher Fryer, Daniel Holz, Emanuele Berti, Tomasz Bulik, Ilya Mandel, and Richard O'Shaughnessy. Double Compact Objects I: The Significance of the Common Envelope on Merger Rates. Astrophys. J., 759:52, 2012.
- [8] Charles D. Bailyn, Raj K. Jain, Paolo Coppi, and Jerome A. Orosz. The Mass distribution of stellar black holes. Astrophys. J., 499:367, 1998.
- [9] B. P. Abbott et al. GWTC-1: A Gravitational-Wave Transient Catalog of Compact Binary Mergers Observed by LIGO and Virgo during the First and Second Observing Runs. *Phys. Rev. X*, 9(3):031040, 2019.
- [10] B. P. Abbott et al. Observation of Gravitational Waves from a Binary Black Hole Merger. *Phys. Rev. Lett.*, 116(6):061102, 2016.
- [11] R. Abbott et al. Population of Merging Compact Binaries Inferred Using Gravitational Waves through GWTC-3. Phys. Rev. X, 13(1):011048, 2023.
- [12] Yann Bouffanais, Michela Mapelli, Filippo Santoliquido, Nicola Giacobbo, Ugo N. Di Carlo, Sara Rastello, M. Celeste Artale, and Giuliano Iorio. New insights on binary black hole formation channels after GWTC-2: young star clusters versus isolated binaries. Mon. Not. Roy. Astron. Soc., 507(4):5224–5235, 2021.
- [13] Gabriele Franciolini, Vishal Baibhav, Valerio De Luca, Ken K. Y. Ng, Kaze W. K. Wong, Emanuele Berti, Paolo Pani, Antonio Riotto, and Salvatore Vitale. Searching for a subpopulation of primordial black holes in LIGO-Virgo gravitational-wave data. *Phys. Rev. D*, 105(8):083526, 2022.
- [14] April Qiu Cheng, Michael Zevin, and Salvatore Vitale. What You Don't Know Can Hurt You: Use and Abuse of Astrophysical Models in Gravitational-wave Population Analyses. Astrophys. J., 955(2):127, 2023.
- [15] Andrea Antonelli, Konstantinos Kritos, Ken K. Y. Ng, Roberto Cotesta, and Emanuele Berti. Classifying the generation and formation channels of individual LIGO-Virgo-KAGRA observations from dynamically formed binaries. *Phys. Rev. D*, 108(8):084044, 2023.
- [16] Kaze W. K. Wong, Katelyn Breivik, Will M. Farr, and Rodrigo Luger. Backward Population Synthesis: Mapping the Evolutionary History of Gravitational-wave Progenitors. Astrophys. J., 950(2):181, June 2023.
- [17] Vaibhav Tiwari and Stephen Fairhurst. The Emergence

- of Structure in the Binary Black Hole Mass Distribution. Astrophys. J. Lett., 913(2):L19, 2021.
- [18] Vaibhav Tiwari. Exploring Features in the Binary Black Hole Population. Astrophys. J., 928(2):155, 2022.
- [19] A. G. Abac et al. Observation of Gravitational Waves from the Coalescence of a 2.5 - 4.5 solar mass Compact Object and a Neutron Star. Astrophys. J. Lett., 970(2):L34, 2024.
- [20] B. P. Abbott et al. Binary Black Hole Mergers in the first Advanced LIGO Observing Run. Phys. Rev. X, 6(4):041015, 2016. [Erratum: Phys.Rev.X 8, 039903 (2018)].
- [21] F. Acernese et al. Advanced Virgo: a second-generation interferometric gravitational wave detector. Class. Quant. Grav., 32(2):024001, 2015.
- [22] T. Akutsu et al. Overview of KAGRA: Detector design and construction history. PTEP, 2021(5):05A101, 2021.
- [23] B. P. Abbott et al. GW170817: Observation of Gravitational Waves from a Binary Neutron Star Inspiral. Phys. Rev. Lett., 119(16):161101, 2017.
- [24] B. D. Metzger and E. Berger. What is the Most Promising Electromagnetic Counterpart of a Neutron Star Binary Merger? Astrophys. J., 746(1):48, February 2012.
- [25] E. Troja et al. The X-ray counterpart to the gravitational wave event GW 170817. Nature, 551:71-74, 2017.
- [26] B. P. Abbott et al. GW170817: Measurements of neutron star radii and equation of state. Phys. Rev. Lett., 121(16):161101, 2018.
- [27] Eanna E. Flanagan and Tanja Hinderer. Constraining neutron star tidal Love numbers with gravitational wave detectors. Phys. Rev. D, 77:021502, 2008.
- [28] Simeon Bird, Ilias Cholis, Julian B. Muñoz, Yacine Ali-Haïmoud, Marc Kamionkowski, Ely D. Kovetz, Alvise Raccanelli, and Adam G. Riess. Did LIGO detect dark matter? Phys. Rev. Lett., 116(20):201301, 2016.
- [29] Sebastien Clesse and Juan García-Bellido. The clustering of massive Primordial Black Holes as Dark Matter: measuring their mass distribution with Advanced LIGO. Phys. Dark Univ., 15:142–147, 2017.
- [30] Misao Sasaki, Teruaki Suyama, Takahiro Tanaka, and Shuichiro Yokoyama. Primordial Black Hole Scenario for the Gravitational-Wave Event GW150914. Phys. Rev. Lett., 117(6):061101, 2016. [Erratum: Phys.Rev.Lett. 121, 059901 (2018)].
- [31] Karsten Jedamzik. Primordial black hole formation during the QCD epoch. Phys. Rev. D, 55:5871–5875, 1997.
- [32] Juan Garcia-Bellido, Andrei D. Linde, and David Wands. Density perturbations and black hole formation in hybrid inflation. *Phys. Rev. D*, 54:6040–6058, 1996.
- [33] Matt Crawford and David N. Schramm. Spontaneous Generation of Density Perturbations in the Early Universe. *Nature*, 298:538–540, 1982.
- [34] Ilia Musco and John C. Miller. Primordial black hole formation in the early universe: critical behaviour and self-similarity. Class. Quant. Grav., 30:145009, 2013.
- [35] Katherine J. Mack, Jeremiah P. Ostriker, and Massimo Ricotti. Growth of structure seeded by primordial black holes. Astrophys. J., 665:1277–1287, 2007.
- [36] Pasquale D. Serpico, Vivian Poulin, Derek Inman, and Kazunori Kohri. Cosmic microwave background bounds on primordial black holes including dark matter halo accretion. *Phys. Rev. Res.*, 2(2):023204, 2020.
- [37] Gabriele Franciolini. Primordial Black Holes: from Theory to Gravitational Wave Observations. PhD thesis, Geneva U., Dept. Theor. Phys., 2021.

- [38] V. De Luca, G. Franciolini, P. Pani, and A. Riotto. The evolution of primordial black holes and their final observable spins. *JCAP*, 04:052, 2020.
- [39] Simon Stevenson and Teagan Clarke. Constraints on the contributions to the observed binary black hole population from individual evolutionary pathways in isolated binary evolution. 10 2022.
- [40] Feng-Hui Zhang, Zhan-Wen Han, Li-Fang Li, and Jarrod R. Hurley. Inclusion of binaries in evolutionary population synthesis. Mon. Not. Roy. Astron. Soc., 357:1088–1103, 2005.
- [41] Ilya Mandel and Alison Farmer. Merging stellar-mass binary black holes. Phys. Rept., 955:1–24, 2022.
- [42] Jordan Barber, Debatri Chattopadhyay, and Fabio Antonini. Black hole binary mergers in dense star clusters: the importance of primordial binaries. 10 2023.
- [43] M. Coleman Miller and Vanessa M. Lauburg. Mergers of Stellar-Mass Black Holes in Nuclear Star Clusters. Astrophys. J., 692:917–923, 2009.
- [44] Giacomo Fragione and Frederic A. Rasio. Demographics of Hierarchical Black Hole Mergers in Dense Star Clusters. Astrophys. J., 951(2):129, 2023.
- [45] Dylan Britt, Ben Johanson, Logan Wood, M. Coleman Miller, and Erez Michaely. Binary black hole mergers from hierarchical triples in open clusters. *Mon. Not.* Roy. Astron. Soc., 505(3):3844–3852, 2021.
- [46] Chase Kimball et al. Evidence for Hierarchical Black Hole Mergers in the Second LIGO-Virgo Gravitational Wave Catalog. Astrophys. J. Lett., 915(2):L35, 2021.
- [47] Robert Farmer, Mathieu Renzo, Selma de Mink, Maya Fishbach, and Stephen Justham. Constraints from gravitational wave detections of binary black hole mergers on the 12 C $(\alpha, \gamma)^{16}$ O rate. Astrophys. J. Lett., 902(2):L36, 2020.
- [48] Piero Madau and Mark Dickinson. Cosmic Star Formation History. Ann. Rev. Astron. Astrophys., 52:415–486, 2014.
- [49] Michal Dominik, Emanuele Berti, Richard O'Shaughnessy, Ilya Mandel, Krzysztof Belczynski, Christopher Fryer, Daniel E. Holz, Tomasz Bulik, and Francesco Pannarale. Double Compact Objects III: Gravitational Wave Detection Rates. Astrophys. J., 806(2):263, 2015.
- [50] Christos Karathanasis, Benoit Revenu, Suvodip Mukherjee, and Federico Stachurski. GWSim: Python package for creating mock GW samples for different astrophysical populations and cosmological models of binary black holes. Astron. Astrophys., 677:A124, 2023. [Erratum: Astron.Astrophys. 682, C1 (2024)].
- [51] Suvodip Mukherjee. The redshift dependence of black hole mass distribution: is it reliable for standard sirens cosmology? Mon. Not. Roy. Astron. Soc., 515(4):5495– 5505, 2022.
- [52] Christos Karathanasis, Suvodip Mukherjee, and Simone Mastrogiovanni. Binary black holes population and cosmology in new lights: signature of PISN mass and formation channel in GWTC-3. Mon. Not. Roy. Astron. Soc., 523(3):4539–4555, 2023.
- [53] Frans Pretorius. Evolution of binary black hole spacetimes. Phys. Rev. Lett., 95:121101, 2005.
- [54] Serguei Ossokine, Tim Dietrich, Evan Foley, Reza Katebi, and Geoffrey Lovelace. Assessing the Energetics of Spinning Binary Black Hole Systems. *Phys. Rev.* D, 98(10):104057, 2018.
- [55] Mark A. Scheel, Michael Boyle, Tony Chu, Lawrence E. Kidder, Keith D. Matthews, and Harald P. Pfeiffer. High-accuracy waveforms for binary black hole inspiral, merger, and ringdown. *Phys. Rev. D*, 79:024003,

- 2009.
- [56] Manuela Campanelli, C. O. Lousto, and Y. Zlochower. Spinning-black-hole binaries: The orbital hang up. Phys. Rev. D, 74:041501, 2006.
- [57] Maya Fishbach, Daniel E. Holz, and Ben Farr. Are LIGO's Black Holes Made From Smaller Black Holes? Astrophys. J. Lett., 840(2):L24, 2017.
- [58] Carl L. Rodriguez, Meagan Morscher, Bharath Pattabiraman, Sourav Chatterjee, Carl-Johan Haster, and Frederic A. Rasio. Binary Black Hole Mergers from Globular Clusters: Implications for Advanced LIGO. Phys. Rev. Lett., 115(5):051101, 2015. [Erratum: Phys.Rev.Lett. 116, 029901 (2016)].
- [59] Jongsuk Hong, Enrico Vesperini, Abbas Askar, Mirek Giersz, Magdalena Szkudlarek, and Tomasz Bulik. Binary Black Hole Mergers from Globular Clusters: the Impact of Globular Cluster Properties. Mon. Not. Roy. Astron. Soc., 480(4):5645–5656, 2018. [Erratum: Mon.Not.Roy.Astron.Soc. 491, 5793 (2020)].
- [60] Ryan M. O'Leary, Bence Kocsis, and Abraham Loeb. Gravitational waves from scattering of stellar-mass black holes in galactic nuclei. Mon. Not. Roy. Astron. Soc., 395(4):2127–2146, 2009.
- [61] Krzysztof Belczynski, Serena Repetto, Daniel E. Holz, Richard O'Shaughnessy, Tomasz Bulik, Emanuele Berti, Christopher Fryer, and Michal Dominik. Compact Binary Merger Rates: Comparison with LIGO/Virgo Upper Limits. Astrophys. J., 819(2):108, 2016.
- [62] Krzysztof Belczynski, Tomasz Bulik, Chris L. Fryer, Ashley Ruiter, Francesca Valsecchi, Jorick S. Vink, and Jarrod R. Hurley. On the Maximum Mass of Stellar Black Holes. Astrophys. J., 714(2):1217–1226, May 2010.
- [63] Michela Mapelli, Nicola Giacobbo, Emanuele Ripamonti, and Mario Spera. The cosmic merger rate of stellar black hole binaries from the Illustris simulation. Mon. Not. Roy. Astron. Soc., 472(2):2422–2435, 2017.
- [64] Mario Spera and Michela Mapelli. Very massive stars, pair-instability supernovae and intermediatemass black holes with the SEVN code. Mon. Not. Roy. Astron. Soc., 470(4):4739–4749, 2017.
- [65] Michela Mapelli. Massive black hole binaries from runaway collisions: the impact of metallicity. Mon. Not. Roy. Astron. Soc., 459(4):3432–3446, 2016.
- [66] Y. Yang, I. Bartos, Z. Haiman, B. Kocsis, S. Márka, and H. Tagawa. Cosmic Evolution of Stellar-mass Black Hole Merger Rate in Active Galactic Nuclei. Astrophys. J., 896(2):138, 2020.
- [67] Jarrod R. Hurley, Christopher A. Tout, and Onno R. Pols. Evolution of binary stars and the effect of tides on binary populations. *Mon. Not. Roy. Astron. Soc.*, 329:897, 2002.
- [68] Fabio Antonini and Frederic A. Rasio. Merging black hole binaries in galactic nuclei: implications for advanced-LIGO detections. Astrophys. J., 831(2):187, 2016.
- [69] Sai Wang, Yi-Fan Wang, Qing-Guo Huang, and Tjonnie G. F. Li. Constraints on the Primordial Black Hole Abundance from the First Advanced LIGO Observation Run Using the Stochastic Gravitational-Wave Background. Phys. Rev. Lett., 120(19):191102, 2018.
- [70] Rong-Gen Cai, Chao Chen, and Chengjie Fu. Primordial black holes and stochastic gravitational wave background from inflation with a noncanonical spectator field. *Phys. Rev. D*, 104(8):083537, 2021.
- [71] Vuk Mandic, Simeon Bird, and Ilias Cholis. Stochastic Gravitational-Wave Background due to Primor-

- dial Binary Black Hole Mergers. *Phys. Rev. Lett.*, 117(20):201102, 2016.
- [72] T. Ertl, S. E. Woosley, Tuguldur Sukhbold, and H. T. Janka. The Explosion of Helium Stars Evolved with Mass Loss. Astrophys. J., 890(1):51, February 2020.
- [73] Conrad Chan, Bernhard Müller, and Alexander Heger. The impact of fallback on the compact remnants and chemical yields of core-collapse supernovae. Mon. Not. Roy. Astron. Soc., 495(4):3751–3762, 2020.
- [74] Benjamin P. Abbott et al. Effects of waveform model systematics on the interpretation of GW150914. Class. Quant. Grav., 34(10):104002, 2017.
- [75] Chris Pankow, Laura Sampson, Leah Perri, Eve Chase, Scott Coughlin, Michael Zevin, and Vassiliki Kalogera. Astrophysical Prior Information and Gravitationalwave Parameter Estimation. Astrophys. J., 834(2):154, 2017.
- [76] Laura Sampson, Neil Cornish, and Nicolás Yunes. Mismodeling in gravitational-wave astronomy: The trouble with templates. Phys. Rev. D, 89(6):064037, 2014.
- [77] David Reitze et al. Cosmic Explorer: The U.S. Contribution to Gravitational-Wave Astronomy beyond LIGO. Bull. Am. Astron. Soc., 51(7):035, 2019.
- [78] Michele Maggiore et al. Science Case for the Einstein Telescope. *JCAP*, 03:050, 2020.
- [79] Monica Colpi et al. LISA Definition Study Report. 2 2024.
- [80] Stefan Van Der Walt, S Chris Colbert, and Gael Varoquaux. The numpy array: a structure for efficient numerical computation. Computing in science & engineering, 13(2):22–30, 2011.
- [81] Eric Jones, Travis Oliphant, Pearu Peterson, et al. SciPy: Open source scientific tools for Python, 2001–. [Online; accessed itoday].
- [82] John D Hunter. Matplotlib: A 2d graphics environment. Computing in science & engineering, 9(03):90–95, 2007.
- [83] Thomas P Robitaille, Erik J Tollerud, Perry Greenfield, Michael Droettboom, Erik Bray, Tom Aldcroft, Matt Davis, Adam Ginsburg, Adrian M Price-Whelan, Wolfgang E Kerzendorf, et al. Astropy: A community python package for astronomy. Astronomy & Astrophysics, 558:A33, 2013.
- [84] Martti Raidal, Christian Spethmann, Ville Vaskonen, and Hardi Veermäe. Formation and Evolution of Primordial Black Hole Binaries in the Early Universe. JCAP, 02:018, 2019.
- [85] Ville Vaskonen and Hardi Veermäe. Lower bound on the primordial black hole merger rate. Phys. Rev. D, 101(4):043015, 2020.
- [86] Yacine Ali-Haïmoud, Ely D. Kovetz, and Marc Kamionkowski. Merger rate of primordial black-hole binaries. Phys. Rev. D, 96(12):123523, 2017.
- [87] Yu N. Eroshenko. Gravitational waves from primordial black holes collisions in binary systems. J. Phys. Conf. Ser., 1051(1):012010, 2018.
- [88] Bernard Carr, Martti Raidal, Tommi Tenkanen, Ville Vaskonen, and Hardi Veermäe. Primordial black hole constraints for extended mass functions. *Phys. Rev. D*, 96(2):023514, 2017.
- [89] Benjamin Horowitz. Revisiting Primordial Black Holes Constraints from Ionization History. 12 2016.
- [90] Bernard Carr and Joseph Silk. Primordial Black Holes as Generators of Cosmic Structures. Mon. Not. Roy. Astron. Soc., 478(3):3756–3775, 2018.
- [91] Alexandre Dolgov and Joseph Silk. Baryon isocurvature fluctuations at small scales and baryonic dark matter. *Phys. Rev. D*, 47:4244–4255, May 1993.

- [92] Anne M. Green. Microlensing and dynamical constraints on primordial black hole dark matter with an extended mass function. *Phys. Rev. D*, 94(6):063530, 2016
- [93] Kristjan Kannike, Luca Marzola, Martti Raidal, and Hardi Veermäe. Single Field Double Inflation and Primordial Black Holes. JCAP, 09:020, 2017.
- [94] Florian Kühnel and Katherine Freese. Constraints on Primordial Black Holes with Extended Mass Functions. Phys. Rev. D, 95(8):083508, 2017.
- [95] Hiromichi Tagawa, Zoltan Haiman, and Bence Kocsis. Formation and Evolution of Compact Object Binaries in AGN Disks. Astrophys. J., 898(1):25, 2020.
- [96] Gaia Fabj and Johan Samsing. Eccentric Mergers in AGN Discs: Influence of the Supermassive Black-Hole on Three-body Interactions. arXiv e-prints, page arXiv:2402.16948, February 2024.
- [97] Yuan-Zhu Wang, Yi-Zhong Fan, Shao-Peng Tang, Ying Qin, and Da-Ming Wei. Mass and effective spin distributions of binary black hole events: Evidence for a population of hierarchical black hole mergers in active galactic nuclei disks. 10 2021.
- [98] Xuejian Shen, Philip F. Hopkins, Claude-André Faucher-Giguère, D. M. Alexander, Gordon T. Richards, Nicholas P. Ross, and R. C. Hickox. The bolometric quasar luminosity function at z = 0-7. Mon. Not. Roy. Astron. Soc., 495(3):3252-3275, 2020.
- [99] Marco Tucci and Marta Volonteri. Constraining supermassive black hole evolution through the continuity equation. Astron. Astrophys., 600:A64, 2017.
- [100] Yoshihiro Ueda, Masayuki Akiyama, Günther Hasinger, Takamitsu Miyaji, and Michael G. Watson. Toward the Standard Population Synthesis Model of the X-Ray Background: Evolution of X-Ray Luminosity and Absorption Functions of Active Galactic Nuclei Including Compton-Thick Populations. Astrophys. J., 786:104, 2014.
- [101] A. Marconi, G. Risaliti, R. Gilli, L. K. Hunt, R. Maiolino, and M. Salvati. Local supermassive black holes, relics of active galactic nuclei and the x-ray background. Mon. Not. Roy. Astron. Soc., 351:169, 2004.
- [102] Yang Yang et al. Hierarchical Black Hole Mergers in Active Galactic Nuclei. Phys. Rev. Lett., 123(18):181101, 2019
- [103] Matthew Mould, Davide Gerosa, Marco Dall'Amico, and Michela Mapelli. One to many: comparing single gravitational-wave events to astrophysical populations. Mon. Not. Roy. Astron. Soc., 525(3):3986-3997, 2023.
- [104] Chase Kimball, Christopher P. L. Berry, and Vicky Kalogera. What GW170729's exceptional mass and spin tells us about its family tree. Res. Notes AAS, 4(1):2, 2020.
- [105] Jeff J. Andrews, Julianne Cronin, Vicky Kalogera, Christopher P. L. Berry, and Andreas Zezas. Targeted Modeling of GW150914's Binary Black Hole Source with Dart_board. Astrophys. J. Lett., 914(2):L32, 2021.
- [106] We do not consider eccentricity and kick velocity in the remaining analysis as it is not well measured from current GW data.
- [107] We have classified into three broad categories for this paper.

Appendix A: Merger Rate of Primordial black holes

Primordial black holes (PBHs) are hypothesized to have formed in the early Universe due to density fluctuations during inflation. Unlike black holes formed from stellar collapse, PBHs can vary significantly in mass and are considered a potential component of dark matter. Their formation scenarios include a collapse in the radiation-dominated era and subsequent dynamics in the matter-dominated era, where they can cluster due to gravitational interactions. Understanding the merger rate of PBHs is crucial for assessing their contribution to GW signals detected by observatories like LVK. These mergers may enhance the detection of GWs, offering insights into the nature of dark matter and the conditions of the early Universe. The merger rate of PBHs is given by [84, 85]

$$\begin{split} dR_0 &= \frac{1.6 \times 10^6}{Gpc^3 \, yr} f_{pbh}^{\frac{53}{37}} \eta^{-\frac{34}{37}} \bigg(\frac{M}{M_\odot}\bigg)^{-\frac{32}{37}} \bigg(\frac{\tau}{t_0}\bigg)^{-\frac{34}{37}} \\ &\times 0.24 \bigg(1 + \frac{2.3 S_{eq}}{f_{pbh}^2}\bigg) \psi(m_1) \psi(m_2) dm_1 dm_2, \end{split} \tag{4}$$

where τ is the time elapsed since the formation of PBHs, t_0 is the current age of the universe, and the term $\left(1+\frac{2.3S_{eq}}{f_{pbh}^2}\right)$ reflects the influence of adiabatic perturbations on the eccentricity of early binaries, with $\sqrt{S_{eq}}=0.0005$ representing the variance of matter perturbation at matter-radiation equality [86, 87]. The parameter f_{PBH} denotes the fraction of dark matter composed of PBHs, η is the symmetric mass ratio, and M is the total mass of the binary. The mass distribution of PBHs, denoted as $\psi(M)$, is crucial for understanding their formation and abundance in the universe. This distribution is normalized so that integrating over all masses yields the total PBH density, reflecting how PBH populations are spread across different mass ranges [88, 89].

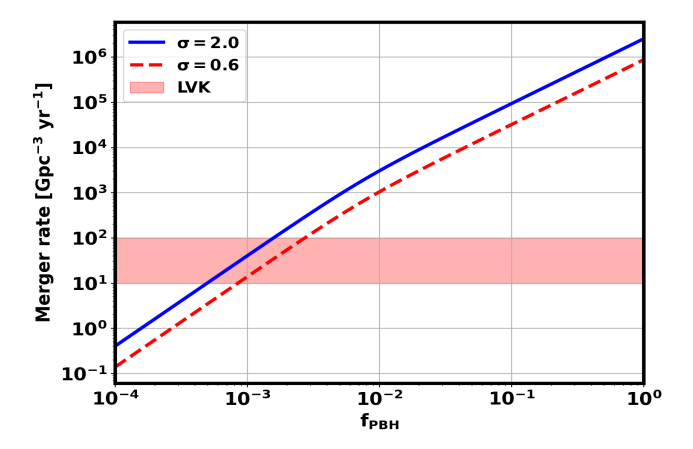


FIG. 3: Integrated merger rate R as a function of f_{PBH} for lognormal mass functions with a characteristic mass $M_c=20\,M_\odot$. The solid blue line represents the lognormal mass function with a width $\sigma=2.0,$ while the dashed red line corresponds to a width $\sigma=0.6.$ The shaded red region indicates the merger rate range consistent with LVK observations

PBH formation is linked to the collapse of density perturbations in the early universe, with their masses determined by the scale of these perturbations. Critical collapse results in a broadening of the mass function, allowing PBHs of varying masses to form simultaneously in different regions. Once formed, PBHs behave like non-relativistic matter, and their abundance evolves differently from the total energy density of the universe, which is dominated by radiation in the early stages. A widely used approximation for this distribution is the log-normal distribution [90]

$$\psi(\mathbf{M}) = \frac{1}{\sqrt{2\pi}\sigma\mathbf{M}} \exp\left[-\frac{\ln^2(\mathbf{M}/\mathbf{M}_c)}{2\sigma^2}\right],\tag{5}$$

where M_c is the characteristic mass and σ defines the width of the distribution. This parameterization allows for easy adjustments to fit observational constraints and explore a wide range of potential PBH populations [91–94].

In Figure 3, we present the integrated merger rate R as a function of the fraction of primordial black holes $f_{\rm PBH},$ using lognormal mass functions characterized by a central mass of $M_c=20\,\rm M_{\odot}.$ The solid blue line illustrates the lognormal mass function with a width of $\sigma=2.0,$ while the dashed red line represents a narrower width of $\sigma=0.6.$ The variation in the width of the mass function affects the overall merger rate, as seen by the distinct behaviors of the two lines. Additionally, the shaded red region highlights the range of merger rates that are consistent with the observations from the LVK collaboration, providing context for the implications of primordial black hole fraction on detectable merger events.

The total number of binary PBH events is expressed as

$$N_{GW} = T_{obs} \int_0^z \frac{dV_c}{dz} \frac{R(z)}{(1+z)} dz,$$
 (6)

where $\frac{\mathrm{d}V_{c}}{\mathrm{d}z}$ represents the differential comoving volume, R(z) is the redshift-dependent merger rate, and T_{obs} is the total observational time in years. The factor (1+z) accounts for the time dilation effect due to cosmic expansion.

Appendix B: Characterizing Mass and Spin of Astrophysical Origin Black Holes

We parameterize the mass function as a combination of a Gaussian and an exponential decay term, allowing it to capture a broader class of mass distributions as defined as follows:

$$P(m) = \begin{cases} \frac{1}{\sqrt{2\pi\sigma^2}} \exp\left(-\frac{(m-M_{mean})^2}{2\sigma^2}\right), & \text{if } m < M_{mean}, \\ \frac{1}{\sqrt{2\pi\sigma^2}} \exp\left(-\frac{(m-M_{mean})^2}{2\sigma^2}\right) & \\ \times \exp(-\alpha(m-M_{mean})), & \text{if } m \ge M_{mean}. \end{cases}$$

The combination of Gaussian and exponential terms allows for flexibility in adapting to various astrophysical mass distributions, effectively capturing both central peaks and tails. The inclusion of the exponential decay term also provides the capability to represent asymmetries in mass distributions, which are common in astrophysical observations. Parameters M_{mean} , σ , and α enable straightforward adjustments to the peak location, width, and decay rate, facilitating alignment with observed data. Each parameter carries clear physical meaning, enhancing discussions about the processes that shape mass distributions.

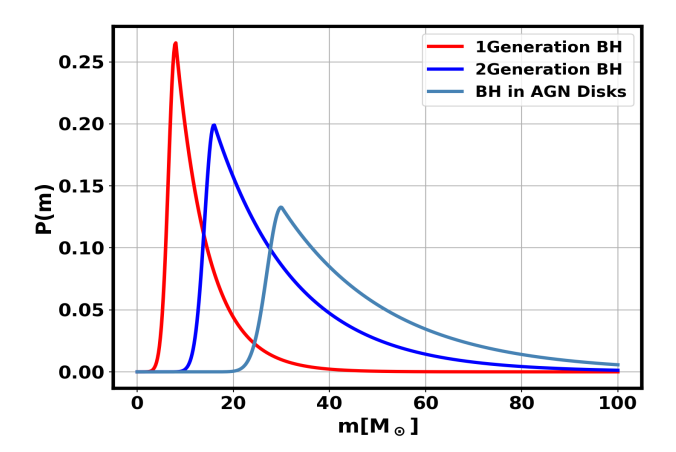


FIG. 4: The probability density functions for first-generation (1G), second-generation (2G) black holes, and black holes in AGN disks are shown. The 1G black holes (red curve) have a peak at 8 M_{\odot} , while the 2G black holes (blue curve) peak at 16 M_{\odot} . Black holes in AGN disks (steel blue curve) are characterized by a peak at 30 M_{\odot} .

In Figure 4, we illustrate the probability density functions for three distinct black hole populations: 1G, 2G, and black holes formed in AGN disks. The red curve represents the mass distribution of 1G black holes, characterized by a peak at 8 M_{\odot} , indicating that the majority of these black holes are clustered around this mass. The blue curve corresponds to 2G black holes, with a higher peak at 16 M_{\odot} , reflecting their larger mass compared to 1G black holes. Finally, the steel blue curve shows the distribution of black holes in AGN disks, which have an even larger peak at 30 M_{\odot} . These differences in mass distributions highlight the varying characteristics of black holes formed through different evolutionary channels.

In the study of binary systems, particularly black holes, the spin parameter χ_1 plays a critical role in understanding merger dynamics. We present a generalized model for the spin parameter as a function of mass, incorporating both mass-dependent growth and saturation mechanisms. The equation is given by:

$$\chi(m) = \left(\frac{m - m_{\min}}{m_{\max} - m_{\min}}\right)^{n} \times \left[1 - \exp\left(-\beta \frac{m - m_{\min}}{m_{\max} - m_{\min}}\right)\right]^{\gamma}, \tag{8}$$

where m_{\min} and m_{\max} define the mass range for spin evolution, n controls the initial spin growth, and β and γ govern the onset and sharpness of spin saturation

at higher masses. This model captures key aspects of black hole spin dynamics, including power-law growth for lower masses and smooth saturation as the mass approaches m_{max} . By constraining the spin within a realistic range, the model provides flexibility for various astrophysical scenarios, from isolated accretion to hierarchical mergers [39–46]. It allows for fine-tuning of the spin evolution by adjusting the parameters, ensuring that the spin behavior remains physically accurate and adaptable to observational data. The spin parameter evolves based on the black hole's mass, reflecting both growth and eventual saturation. This framework is valuable for interpreting gravitational wave detections and other astrophysical signals, enabling better constraints on the spin distribution of black holes and their formation pathways.

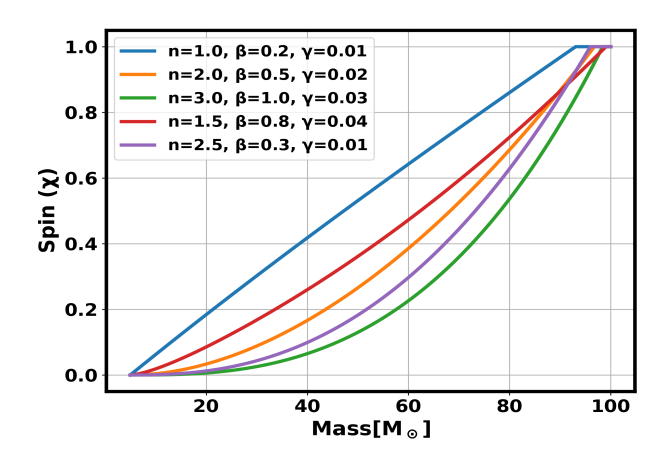


FIG. 5: Plot of the spin parameter $\chi(m)$ as a function of mass(m) for varying parameter values n, β , and γ . This illustrates how adjustments in these parameters influence the growth and saturation behavior of the spin parameter in black holes.

In Figure 5, we present the spin parameter $\chi(m)$ as a function of mass m for varying values of the parameters n, β , and γ . The plot illustrates how changes in these parameters influence the spin growth and its eventual saturation as the black hole mass increases. Specifically, higher values of n tend to delay the onset of spin saturation, while variations in β and γ modulate both the rate of spin growth and the maximum achievable spin. This figure highlights the complex dependence of the spin parameter on both mass and the underlying physical parameters governing black hole formation and evolution.

Appendix C: Merger rate of BBHs using delay time distribution

In the delay time model, the merger rate of BBHs is characterized by the delay time distribution, denoted as t_d . The delay time refers to the elapsed period between the formation of stars that ultimately evolve into black holes and the subsequent merging of these black holes. Importantly, this time delay is not uniform across

all BBHs but rather follows a specific distribution that accounts for the variability in delay times. This distribution function is defined as follows [49–52]:

$$\mathbf{p_t}(\mathbf{t_d}|\mathbf{t_d^{\min}},\mathbf{t_d^{\max}},\mathbf{d}) \propto \begin{cases} (t_d)^{-d} & \text{, for } t_d^{\min} < t_d < t_d^{\max}, \\ 0 & \text{otherwise,} \end{cases}$$

here, the delay time is given by $t_d = t_m - t_f$, where t_m and t_f represent the lookback times of the merger and formation, respectively.

For the 1G BBH merger rate at a given redshift z, we can express it as:

$$R_{1G}(z) = R_0 \frac{\int_z^{\infty} p_t(t_d | t_d^{\min}, t_d^{\max}, d) R_{SFR}(z_f) \frac{dt}{dz_f} dz_f}{\int_0^{\infty} p_t(t_d | t_d^{\min}, t_d^{\max}, d) R_{SFR}(z_f) \frac{dt}{dz_f} dz_f}.$$
(10)

In this equation, the parameter R_0 denotes the local merger rate, which indicates the frequency of mergers at redshift z=0. According to the study by [11], the estimated values of R_0 for the BBH merger rate range between 17.9 ${\rm Gpc}^{-3}\,{\rm yr}^{-1}$ and 44 ${\rm Gpc}^{-3}\,{\rm yr}^{-1}$ at a fiducial redshift of z=0.2. In our analysis, we adopt a standard local merger rate of $R_0=20\,{\rm Gpc}^{-3}\,{\rm yr}^{-1}$ for the BBH system. Here, $R_{SFR}(z_f)$ denotes the star formation rate [48], and $\frac{dt}{dz_f}$ represents the Jacobian of the transformation from cosmic time to redshift.

For the 2G BBHs, which are formed from the mergers of two 1G black holes, we consider a simple model that relies on the formation of the 1G black holes. Similarly utilizing a model motivated by the delay time distributions, we write

$$R_{2G}(z) = R_0 \frac{\int_{z}^{\infty} p_t(t_d | t_d^{\min}, t_d^{\max}, d) R_{1G}(z_f) \frac{dt}{dz_f} dz_f}{\int_{0}^{\infty} p_t(t_d | t_d^{\min}, t_d^{\min}, d) R_{1G}(z_f) \frac{dt}{dz_f} dz_f}.$$
(11)

In this context, the delay time model for 2G black holes is based on the merger rates of 1G BBHs $R_{1G}(z_f)$. We once again employ a delay time distribution model that corresponds to the 1G mergers. This methodology leads to the suppression of the 2G merger rate, which is shifted towards lower redshifts. This behavior effectively reflects the dynamics of black hole mergers across different generations. However, for any other form of the merger rate, one can construct the BCO Phase Space.

In Figure 6, we depict the delay time merger rates for 1G and 2G black holes. The delay time represents the period between the formation of the black hole binary and their eventual merger. For 1G black holes, the delay time is set at 500 million years (Myrs), as indicated by the corresponding curve. In contrast, 2G black holes exhibit a longer delay time, with mergers occurring around 1 billion years (Gyr). The figure highlights the temporal difference between the two populations, with 2G black holes typically experiencing longer periods before merging compared to their 1G counterparts.

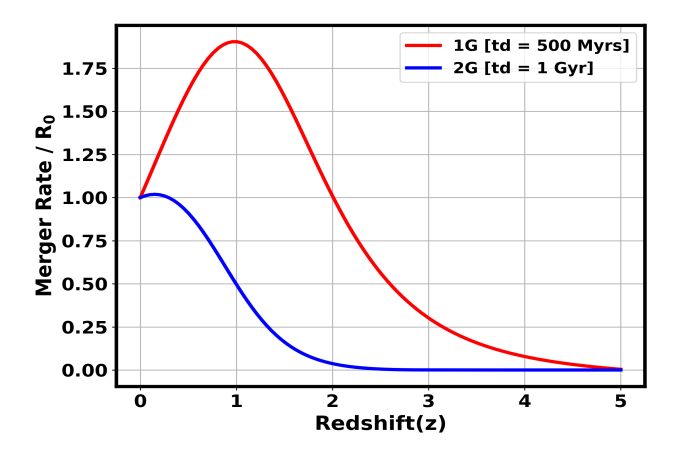


FIG. 6: The figure shows the delay time merger rates for first-generation (1G) and second-generation (2G) black holes. The delay time for 1G black holes is set at 500 Myrs, while for 2G black holes it is set at 1 Gyr.

$\begin{array}{c} \textbf{Appendix D:} \textbf{Merger Rate of black holes in AGN} \\ \textbf{Disks} \end{array}$

The active galactic nucleus (AGN) disk environment offers a unique setting where black hole mergers can occur at an elevated rate compared to other astrophysical scenarios. The dense gas in AGN disks fosters both black hole growth through accretion and dynamical interactions that lead to frequent mergers. In such environments, the high density of stellar-mass black holes within the disk promotes the formation of binaries that can merge due to gas torques, gravitational wave emission, and multi-body interactions. The presence of this gas-rich medium not only accelerates black hole mass growth via accretion but also increases the probability of repeated mergers, especially among lower-mass black holes that can evolve into more massive systems [95–97].

The rate of black hole mergers in AGN disks is significantly enhanced because the gas drives black holes toward the disk midplane, where they become trapped and accumulate in large numbers. As black holes interact within this high-density region, the probability of binary formation and subsequent mergers increases. A key factor determining the black hole merger rate in AGN disks is the population density of AGNs, which evolves with redshift. This density can be constrained using the AGN luminosity function (LF), $f_L(L,z)$, which describes the distribution of AGNs as a function of their luminosity and redshift. The bolometric AGN LF provides insights into the overall energy output of AGNs, which is related to the number of black holes in their disks capable of undergoing mergers, can be expressed as [98]:

$$f_L(L,z) = \frac{f_*(L)}{\left(\frac{L}{L_*}\right)^{\gamma_1(z)} + \left(\frac{L}{L_*}\right)^{\gamma_2(z)}},$$
 (12)

where $\gamma_1(z)$, $\gamma_2(z)$, and $L_*(z)$ are given by the following relations:

$$\gamma_1(z) = \alpha_0 T_0(1+z) + \alpha_1 T_1(1+z) + \alpha_2 T_2(1+z), (13)$$

$$\gamma_2(z) = \frac{2b_0}{\left(\frac{1+z}{3}\right)^{b_1} + \left(\frac{1+z}{3}\right)^{b_2}},\tag{14}$$

$$\log L_*(z) = \frac{2c_0}{\left(\frac{1+z}{3}\right)^{c_1} + \left(\frac{1+z}{3}\right)^{c_2}},\tag{15}$$

$$\log f_*(z) = d_0 T_0(1+z) + d_1 T_1(1+z), \tag{16}$$

where $T_n(z)$ are Chebyshev polynomials. The best-fit parameters are listed in the Table II.

α_0	α_1	α_2	β_0	β_1	β_2	c_0	c_1	c_2	d_0	d_1
0.8396	-0.2519	0.0198	2.5432	-1.0528	1.1284	13.0124	-0.5777	0.4545	-3.5148	-0.4045

TABLE II: Best Fit Parameter Values for the AGN Luminosity Function

The AGN density $n_{\text{AGN}}(z)$ can be obtained through direct integration of $f_L(L,z)$ with a lower cutoff L_{min} due to large uncertainties. The mass of supermassive black holes (SMBHs) correlates with AGN luminosity via:

$$\frac{M_{\bullet}}{M_{\odot}} = 3.17 \times 10^{-5} \frac{1-\epsilon}{\dot{m}} \frac{L}{L_{\odot}}, \tag{17} \label{eq:model}$$

where ϵ is the radiation efficiency and \dot{M} is the SMBH accretion rate. This relationship can be reformulated to link the normalized accretion rate \dot{m} with the Eddington ratio $\lambda = L/L_{\rm Edd}$. The Eddington ratio distribution is expressed as a mixture model [99]:

$$P(\lambda|L,z) = f_{\text{uno}}P_1(\lambda|z) + f_{\text{obs}}P_2(\lambda|z), \qquad (18)$$

where $f_{\text{uno}} = 1 - f_{\text{obs}}$ is the fraction of unobscured (type-1) AGNs and f_{obs} the fraction of obscured (type-2) AGNs. For type-1 AGNs, $P_1(\lambda|z)$ follows a log-normal distribution with:

$$\ln \lambda_{\rm c}(z) = \max \left[1.9 - 0.45z, \ln 0.03 \right],\tag{19}$$

$$\sigma_z = \max[1.03 - 0.15z, 0.6]. \tag{20}$$

For type-2 AGNs, $P_2(\lambda|z)$ follows a gamma distribution with a low-Eddington cutoff

$$P_2(\lambda|z) = N_2(z)\lambda^{\alpha(z)} \exp(-\lambda/\lambda_0), \tag{21}$$

where $\lambda_0 = 1.5$, and $\alpha(z)$ is defined as 0.6 for z < 0.6 and 0.4 + 0.6(z - 0.6) for $z \ge 0.6$. The fraction of obscured AGNs, $f_{\rm obs}$, is parameterized as [100]

$$f_{\text{obs}} = \frac{(1 + f_{\text{CTK}})\psi(L_X, z)}{1 + f_{\text{CTK}}\psi(L_X, z)},$$
 (22)

where $f_{\text{CTK}} = 1$ is the ratio of Compton-thick to Compton-thin AGNs, and $\psi(L_X, z)$ is given by

$$\psi(L_X, z) = \min(\psi_{\text{max}}, \beta(\log L_X - 43.75\xi(z)) + \psi_{\text{min}}),$$
(23)

with $\psi_{\rm max}=0.84$, $\psi_{\rm min}=0.2$, $\beta=0.24$, and $\xi(z)=0.43(1+z)^{0.48}$ [101]. The black hole merger rate Γ in a single AGN disk depends on the number of stellar black holes in the disk, $N_{\rm disk}$, which follows

$$N_{\text{disk}}(n_i) = 5.5 n_i^{1/3},$$
 (24)

where n_i is the dominant factor. The average BH merger rate is

$$\Gamma(n_i) = \left(1 - e^{-N_{\text{disk}}(n_i)}\right) / T_{\text{AGN}}, \tag{25}$$

where $T_{\text{AGN}} = 10^7$ years is the AGN lifetime [102]. Assuming that black holes in AGN disks hierarchically merge in migration traps, the BH merger rate becomes

$$\Gamma(\dot{m}) = N_{\text{disk}}(\dot{m}) \frac{1}{T_{\text{AGN}}} (1 - e^{-N_{\text{disk}}(\dot{m})}). \tag{26}$$

Combining these factors, the cosmic black hole merger rate in AGNs as a function of redshift is given by:

$$R_{\rm AGN}(z) = \int_{L_{\rm min}}^{L_{\rm max}} f_L(L, z) \, d \log L \int_{\lambda} P(\lambda | L, z) \, \Gamma(\dot{m}) \, d\lambda.$$
(27)

We use the above expression for calculating the BBH mergers rate redshift evolution hosted in AGNs.

Appendix E:Framework for Phase Space Generation and Identifying Binary Formation Channels

In this section, we describe the basic framework of the BCO Phase Space. Although our full analysis utilizes a three-dimensional phase space, we use a two-dimensional phase space for illustration purposes to improve visual clarity. In this example, we label the variables in this 2D space as X and Y, which could represent any observable parameters that are influenced by the formation channel of a binary system. When these variables are

measured, they correspond to some type of probability distribution. For the purpose of explaining, we assume an asymmetric Gaussian distribution for both the X and Y variables. This creates a 2D phase space as shown in Figure 7, where the phase space is weighted according to the measurement uncertainties.

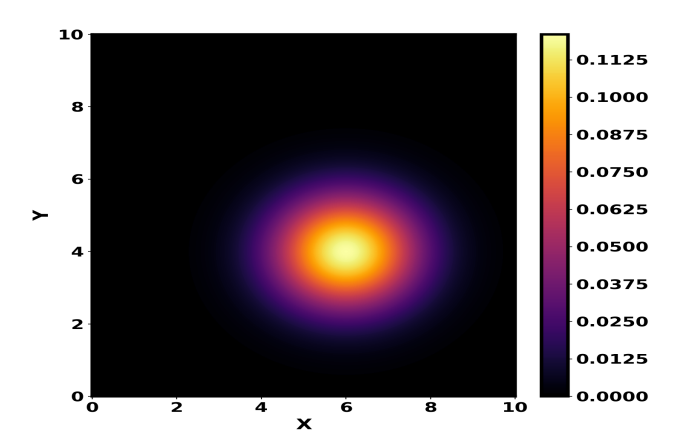


FIG. 7: Representation of the 2D phase space assuming an asymmetric Gaussian distribution for the X and Y variables. The phase space is weighted based on measurement uncertainties, highlighting the distribution of observed data within the defined confidence intervals.

Now, when multiple GW events are analyzed, each event will occupy a different region of the phase space due to its unique measurements and associated uncertainties. As an example, in Figure 8, we generate 10 different GW events, each represented as a confidence interval region in the phase space. From Figure 8, it is clear that there is some overlap between the phase space regions of different events. When multiple events have overlapping regions, we sum the weights in these areas, which are derived from the uncertainties in the measurements of each event. This aggregated phase space, where the weights from multiple events are combined, reflects the total probability distribution over the phase space, as shown in Figure 10.

Finally, to extract information about the formation channels, we project theoretical trajectories onto the observed phase space. These trajectories represent different formation channel models and evolve within the phase space according to their physical characteristics. For the purpose of demonstrating the technique using a simple example, we focus on a two-dimensional projection using the variables X and Y for a toy example, with the trajectories governed by the following function:

$$f(X, a) = \frac{X^a}{20} + 1, \tag{28}$$

a is a parameter that defines the curvature of the trajectory. By plotting these trajectories within the phase space, we can identify regions where they intersect with the observed data. The weighted overlap between the theoretical trajectories and the observed phase space which we define as the projection of the formation channel provides insight into the probability of each specific

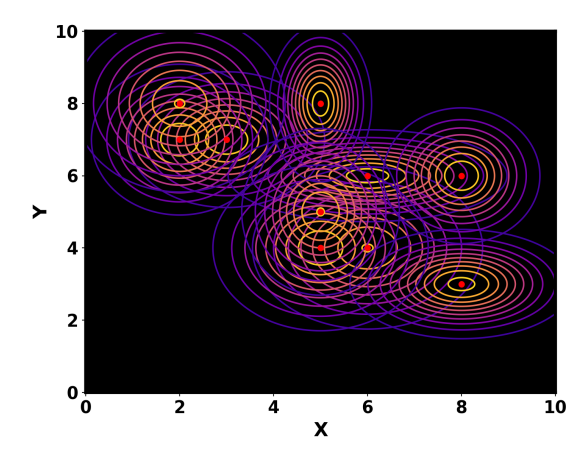


FIG. 8: Visualization of 10 different GW events, each occupying distinct regions of the phase space. Each region represents the confidence interval associated with the unique measurements and uncertainties of each event.

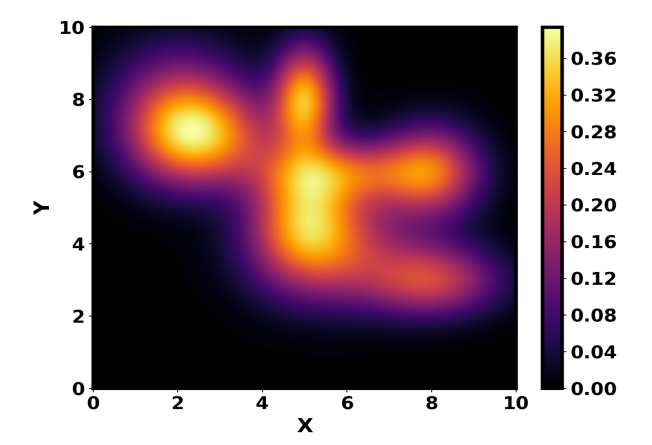


FIG. 9: Visualization of the total weighted phase space constructed from 10 simulated GW events, demonstrating the cumulative contribution of each event to the phase space.

formation channel. However, it is important to note that not all phase space trajectories are detectable by GW observatories. Certain parameter values may fall outside the sensitivity range of the detectors. To account for this, we apply a selection function, S(X,Y), to the model's phase space trajectory, which effectively filters out regions that are inaccessible to the detectors. In a real scenario, the dimensions X and Y can be replaced by parameters such as mass and distance, as GW detectors are most sensitive to these variables. For simplicity, in this example, we define the selection function as S(X,Y)=1, meaning all parameter values are considered allowed.

The projection of various formation channel trajectories onto the observed phase space is illustrated in Figure 10. These trajectories are color-coded according to different values of a, with the weight of each trajectory calculated by summing the phase space values along the curve. This weight reflects the total contribution of each trajectory to the observed phase space, enabling us

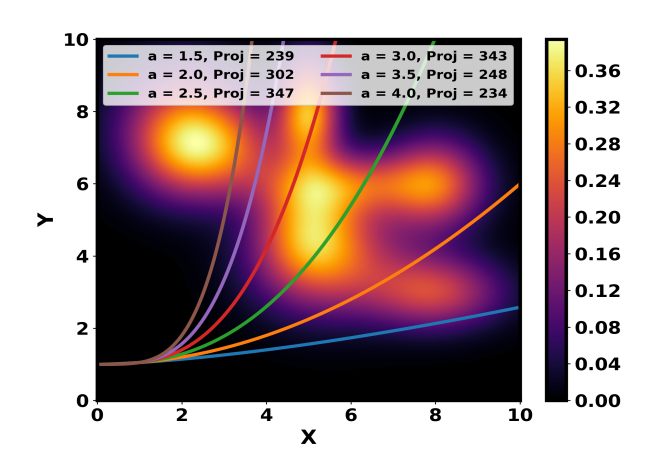


FIG. 10: Projection of theoretical trajectories onto the observed phase space, with color-coded curves representing different curvature values. This plot indicates the probability of various formation channels based on their overlap with the observed data.

to identify the most probable formation channels based on the measured GW events. This projection technique facilitates a quantitative comparison of the probability of different formation channels, enhancing our ability to disentangle the various processes contributing to the observed binary systems. Importantly, this method is applicable to phase spaces of any dimension, making it a versatile tool for analyzing complex systems across a wide range of contexts.

Appendix F: Classification of Compact Binary Events by Formation Channel

We investigate the classification of GW events based on their mass characteristics. This classification is crucial for understanding the potential origins of these events, particularly in distinguishing between different BBH formation channels [103–105]. As illustrated in Figure 11, we categorize each compact binary event from the GWTC-3 catalog, including GW230529, while excluding GW170817, which has been confirmed as a binary neutron star (BNS) system due to its observed electromagnetic counterpart [23].

In Figure 11, each pie chart depicts the probabilities of each event originating from 1G BBH formation channels or a combined category of 2G BBHs and BBHs formed in AGN disks (denoted as 2G+AGN). The top right portion of each pie chart represents the probability of 1G origins, while the left portion indicates the probability of 2G+AGN origins. Events that exhibit a significant probability contribution from either the 1G or the combined 2G+AGN categories are marked in black, indicating a stronger probability of belonging to these channels. In contrast, events with negligible contributions are highlighted in gray indicating them as confusing sources, suggesting they may be potential PBH candidates or channels associated with binary neutron stars which are not

considered in this analysis. The overlaid numbers for these events represent the $M_{\rm int}$ and \dot{m} values for which the event could be considered a candidate for PBH. Note that these values represent only one possible combination; many other combinations are also possible.

To calculate the probability that a BCO event originates from different formation channels, we model the mass distribution for three distinct black hole populations: 1G black holes, 2G black holes, and black holes in AGN disks using a power-law plus Gaussian component as detailed in Equation 7, with distinct parameter values for each formation channel.

For 1G black holes, the mass distribution is characterized by the following parameters: $M_{\rm mean}=8\,M_{\odot},\,\sigma=1.5\,M_{\odot},\,\alpha=0.15.$ For 2G black holes, the parameters are: $M_{\rm mean}=16\,M_{\odot},\,\sigma=2.0\,M_{\odot},\,\alpha=0.06.$ For black holes in AGN disks, the mass distribution is given by: $M_{\rm mean}=30\,M_{\odot},\,\sigma=2.5\,M_{\odot},\,\alpha=0.05.$ The probability distribution of the chirp mass $P(M_{\rm chirp})$ is then computed by marginalizing over the mass distributions of the two individual black holes in the binary system. The chirp mass M_c is related to the component masses m_1 and m_2 by:

$$M_{c} = \frac{(m_1 m_2)^{3/5}}{(m_1 + m_2)^{1/5}}$$
 (29)

To calculate the chirp mass distribution $P(M_c)$, we integrate over the mass distributions $P(m_1)$ and $P(m_2)$ of the two component black holes:

$$P(M_c) = \int \int P(m_1)P(m_2) \times \delta \left(M_c - \frac{(m_1 m_2)^{3/5}}{(m_1 + m_2)^{1/5}} \right) dm_1 dm_2$$
(30)

where δ is the Dirac delta function, ensuring that only the correct combinations of m_1 and m_2 contribute to the chirp mass M_c . Finally, to compute the probability that an observed binary event originates from a particular formation channel, we use the following expression for the probability w_{channel} :

$$w_{channel} = \frac{\int P_{event}(M_c) P_{channel}(M_{chirp}) dM_{chirp}}{\int P_{channel}(M_{chirp}) dM_{chirp}}. \quad (31)$$

Here, $P_{\text{event}}(M_{\text{chirp}})$ represents the likelihood of chirp mass of the observed event, and $P_{\text{channel}}(M_{\text{chirp}})$ represents the mass distribution for a specific formation channel. The integration is performed over the entire range of chirp masses M_{chirp} .

In the catalog, there are six events (GW190425, GW190814, GW190917, GW191219, GW200115, and GW230529) that are unlikely to originate from standard BBH formation channels, as they exhibit relatively lower masses. Additionally, the overlaid numbers on the pie charts correspond to the values of M_{int} and m for these events, indicating the conditions under which they could be considered PBH candidates. For this plot, we

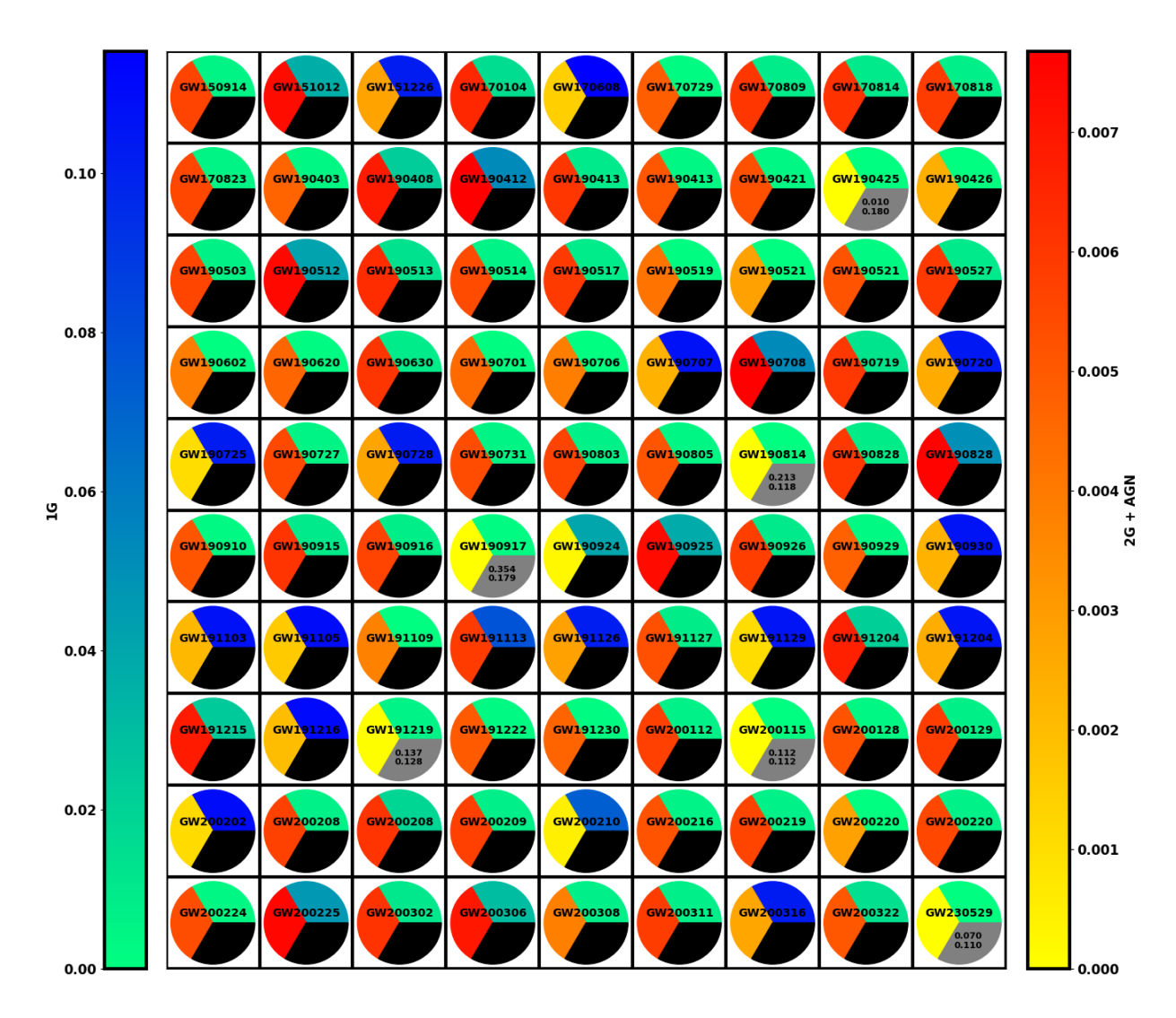


FIG. 11: This figure displays the probabilities of each compact binary event from GWTC-3 and GW230529 (excluding GW170817, which is confirmed to be a BNS system [23]) originating from either 1G BBH or 2G BBH combined with BBH in AGN disks (2G+AGN) formation channels. Each pie chart represents the relative probabilities of the event being of 1G (top right side) and 2G+AGN (left side) origin. For events with significant probability contributions from either 1G or 2G+AGN, the lower portion of the pie is shown in black, while for events with negligible probability contributions, it is shown in gray for the *confusing sources*. The overlaid numbers for these events represent the $M_{\rm int}$ (top) and \dot{m} (below) values for which the event could be considered a candidate for PBH. Note that these values represent only one possible combination; many other combinations are also possible.

have utilized the same probability distributions as employed in Figure 1, with the same parameters. While these probabilities may vary if we adjust the parameters, it is unlikely that changes would significantly impact the classification of these six events due to their sufficiently low mass. It is important to note that the values displayed represent only one possible combination; various other combinations are also feasible. While the probability of an event originating from a particular formation channel may shift with changes in the parameters governing the formation channels, it is unlikely that the classification of these six events would be significantly affected. These events are positioned at the lower end of the mass spectrum, making it improbable that they originate from any standard astrophysical formation channel. Thus, even with parameter variations, their classification remains robust. An alternative explanation for these events could involve the formation of second-generation BBHs from the merger of two neutron stars or other compact objects. The BCO Phase Space study of binaries with neutron stars will be explored in future work.